# Investigation of Fleural Properties of Glued Laminated Timber Composed of Oil Palm Wood

Martin Hackel
Technische Hochschule Ostwestfalen-Lippe
Lemgo, Deutschland

# Investigation of Fleural Properties of Glued Laminated Timber Composed of Oil Palm Wood

## 1. Introduction

As global population increases, raw material consumption rises. The main drivers of this development are the food industry, energy sector, chemical and pharmaceutical industry as well as the construction sector. Oil palms (*Elaeis guineensis* JACQ.) supply all these industries with raw material. The increased material consumption has led to an expansion of oil palm cultivation areas, especially in Southeast Asia. Between 1995 and 2020, the cultivation area increased by 350 % to 28.7 million hectares [1]. The economic lifespan of oil palms is limited to approximately 25 – 30 years [2]. The clearing of plantation areas after the economic lifespan results in about 100 million m³ usable oil palm wood per year [2]. The accumulated material is only used to a limited extent. The material has the potential for substituting tropical timbers, for example, as raw material for building products in its areas of cultivation.
The development of building products based on wood or other lignified plants (palms, bamboo) is an economically costly process. Use cases, production and properties of building products are specified in the European Union and worldwide by corresponding standards (Glulam: DIN EN 408:2012-10 [3], DIN EN 14080:2013-09 [4]). To show compliance, respective tests need to be carried out. These tests are associated with a significant economic effort.
Digitalisation and improvements in computer science offer opportunities to reduce the economic effort of developing building products. In this context, the finite element method (FEM) is a common tool. Using FEM, larger test series can be performed by varying the input data of a predefined model and time and material consumption can be reduced. The application quality of the FEM depends on the quality of the material and experiment parameters used for modelling. In the literature, necessary material characteristics for oil palm wood are limited. As a result, no modelling of products made of oil palm wood has been carried out to date.
The objective of this work is to examine the suitability of the FEM for modelling the flexural behaviour of glulam beams made of oil palm wood. Based on the examination of literature on the modelling of layered materials and elastic constants of oil palm wood, methods for modelling oil palm glulam beams are developed. The methods are implemented and the results compared with laboratory tests. Local and global bending modulus of elasticity (MOE) and correlations between MOE and density of the specimens are determined. Influences of model parameters are to be examined. Representation dimension (two- / three-dimensional), underlying material model (isotropic linear elastic / orthotropic linear elastic), riders in the support situation, material properties (destructive / non-destructive material testing) and element size are the focussed parameters. The significance of the influencing factors is investigated. The suitability of the software RFEM 6.02 (Dlubal Software GmbH) for the given task is evaluated.

## 2. State of the Art

The following sections provide an overview of the state of knowledge in the fields of oil palm wood with its anatomical, physical and mechanical characteristics relevant for modelling and the application of the FEM for layer-based wooden and composite materials.

### 2.1. Anatomical features of oil palm wood

Oil palms (*Elaeis guineensis* JACQ.) are monocotyledons. Their anatomical structure differs from conifers and deciduous trees (dicotyledons). Oil palms lack various features typical for

dicotyledons, for example annual rings, wood rays, a differentiation between heartwood and sapwood, knots, fibre deviations and other inhomogeneities. The tissue is considered anisotropic. Differences between radial and tangential direction do not occur [5, 6].
On a macroscopic level, the tissue of the oil palm (oil palm wood) consists of two structural features, low-density parenchymatic ground tissue and high-density vascular bundles. The vascular bundles run mostly parallel to the surface of the trunk. Killmann and Lim [5] report helically running vascular bundles in the upper part of the trunk. The distribution of vascular bundles within the trunk influences the properties of the oil palm wood. Starting from the trunk periphery, the stem is characterised by a 15 - 26 mm thick layer of parenchymatous ground tissue with irregular fibre strands and undirected vascular bundles, referred to as the cortex. This structure differs from the internal zones of the trunks [5]. Lim and Khoo [2] define three zones. The outer zone occupies approximately 20 % of the stem cross section. It is characterised by a low proportion of parenchymatous tissue and a high vascular bundles content [5]. The inner zone occupies about 40 % of the stem cross section and is characterised by scattered larger vascular bundles. The central zone represents a transitional area between peripheral and inner zone. It occupies 40% of the stem cross section [7]. Fathi [8] confirms this relationship and describes a decreases of vascular bundles towards the inner zone. Lim and Khoo [2] report a correlation between stem height and the proportion of vascular bundles per unit area. Fathi [8] confirms the results of Lim and Khoo [6].
The density is crucial for the elastic properties of oil palm wood. The density of oil palm wood varies significantly depending on its position in the trunk. Lim and Khoo [6] indicate a density range of 170 - 700 kg/m³ and report a correlation between proportion of vascular bundles and density. Within the horizontal plane the density increases with increasing distance from the stem centre. Density decreases with increasing stem height [5, 6, 8]. Kölli [7] describes the variation of the density along the stem axis and in the horizontal direction using exponential functions.

## 2.2. Elastic constants of oil palm wood

The material behaviour of oil palm wood in the linear elastic range can be described using nine elastic constants. The constants are the Young´s moduli (E) along the three anatomical axes, three shear moduli in the symmetry planes (G) and three Poisson`s ratios (μ). Fruehwald-Koenig [9] uses ultrasonic measurements to determine the dynamic MOE in the direction of the vascular bundles. The results exceed the results of static bending tests and show linear correlation with the density ($R^2 = 0.81$). Fruehwald-Koenig and Heister [10] determine a Young´s modulus in tension parallel to the vascular bundles of 488 – 13102 MPa and report an exponential relationship between density and tensile Young´s modulus ($R^2 = 0.53$).
Kölli [11] determines shear moduli $G_{TL}$ and $G_{RL}$ in static tests and shows linear ($R^2 = 0.39$) or exponential relationships ($R^2 = 0.43$) between density and shear modulus. Fruehwald-Koenig and Faust [12] determine the shear modulus in all three planes using dynamic ultrasonic measurements. The results of $G_{LR}$ and $G_{TL}$ show a correlation ($R^2 = 0.87$) to the density, whereas for $G_{RT}$ the correlation is weaker ($R^2 = 0.56$).
Poisson's ratios are determined by Fruehwald-Koenig and Faust [12] using ultrasonic measurements ($\mu_{LR} = 0.389$, $\mu_{RL} = 0.026$, $\mu_{LT} = 0.911$, $\mu_{TL} = 0.044$, $\mu_{RT} = 0.647$ and $\mu_{TR} = 0.707$). Hackel [13] determines Poisson's ratios in compression tests, using digital image correlation. Radial and tangential direction are not differentiated. The ratios $\mu_{LR/T} = 0.379 - 0.523$ are obtained. There are no correlations between density and Poisson's ratio ($R^2 = 0.0024$). In a separate evaluation on the test specimen, a ratio of $\mu_{RT} = 0.117$ is obtained.

## 2.3. FEM for layered wooden materials

The use of the FEM is an established technique for modelling the flexural behaviour of glulam beams and other layered wooden materials. One of the first applications of FEM to predict the load-bearing capacity of spruce glulam beams is presented by Ehlbeck *et al.* [14]. In a two-step process, the structure of the beams with varying material properties and inhomogeneities is generated and then the load-bearing capacity is calculated using the FEM. Linear-elastic material behaviour is assigned to the elements in the tension zone

and ideal plastic behaviour to the compression zone. If the tensile strength within an element is reached, a failure of the element is assumed. If the compressive strength is exceeded, the properties of the elements are changed so that no further forces can be absorbed [14]. An improvement of the approach of Ehlbeck *et al.* [14] («Karlsruhe calculation model») and transfer to beech wood is carried out by Blaß *et al.* [15, pp. 58-61]. The model is formed analogous to Ehlbeck *et al.* [14]. In the first stage, the production of glulam lamellas with stochastically distributed properties is simulated. The modelling of a four-point bending test (DIN EN 408:2004-08) using FEM to determine the MOE and the bending strength forms the second stage [15, 16]. The possibility of applying the described method to other wood species is discussed by Gao *et al.* [17], using the wood species Cathay Poplar. Compared to real tests on corresponding glulam beams, the MOE is overestimated with FEM, but the bending strength is underestimated [17].
Further, FEM can be used to model the flexural behaviour of hybrid glulam beams. Ferrier *et al.* [18] use FEM to investigate glulam beams made of wood, concrete and carbon fibre reinforced plastic. The individual zones of the model (wood, concrete, plastics) are assigned to material parameters corresponding to the material behaviour. The connection between the materials is assumed to be a perfect bond. The model is compared with laboratory tests. Load-displacement diagrams of modelling and laboratory tests show good agreement.

# 3. Material

The test specimen modelled in this work are layered beams produced and physically tested by Heister [19]. The properties of the lamellae used to set up the beams vary over the height of the beam. The dimensions of the beams are 2200 mm x 50 mm x 102 mm (length x width x height). The beams consist of six 17 mm thick lamellae. The properties of the lamellae are selected so that the beams achieve strength class C 14 (DIN EN 338:2016-07 [20]) and the extrapolated strength class C 10 defined by Heister [19]. Densities and other material properties are assigned to the three zones of the beam (tension, shear, compression). The density range for tension lamellae is set to 335 – 363 kg/m³ (C 10) and > 427 kg/m³ (C 14). The compression zone density ranges are 289 – 335 kg/m³ (C 10) and 363 - 427 kg/m³ (C 14). In the shear zone lamellae show densities < 289 kg/m³ (C 10, C 14). Two types of lamellas were used to build up the GLT beams: Specimens with the identification N (natural) are composed of inhomogeneous lamellae showing natural property gradients. Specimens with the identification A (assembled) are formed of lamellae manufactured from narrow stripes of homogeneous density showing reduced property gradients.

## 3.1. Determination of the material parameters

The Young´s moduli and shear moduli are calculated with regression functions between density and the corresponding material constants. Fruehwald-Koenig and Faust [12] provide relationships shown in equation (1) – (3) for Young´s moduli along the anatomical axes and in equation (4) – (6) for the shear moduli in the symmetry planes (all determined from ultrasonic testing).

$$E_L(\rho) = 22.345\,\rho + 204.89 \quad (1)$$

$$E_R(\rho) = 0.318\,\rho + 223.38 \quad (2)$$

$$E_T(\rho) = 1.37\,\rho - 42.164 \quad (3)$$

$$G_{RT}(\rho) = 0.6917\,\rho - 16.657 \quad (4)$$

$$G_{TL}(\rho) = 1.3857\,\rho - 91.621 \quad (5)$$

$$G_{LR}(\rho) = 1.0738\,\rho - 37.963 \quad (6)$$

$E_{L,R,T} = Young´s\ moduli\ along\ the\ anatomical\ axes\ [MPa], G_{RT,TL,LR} = shear\ moduli\ in\ the\ symmetry\ planes\ [MPa], \rho = density\ [\frac{kg}{m^3}]$

Fruehwald-Koenig and Heister [10] determine the relationship between density and Young´s modulus parallel to the vascular bundles shown in equation (7) using static tensile tests. Respectively, equation (8) shows the relationship between density and shear modulus in the TL plane longitudinal direction determined by Kölli [11] in a two-plate shear test.

$$E_{t,0}(\rho) = 0.0021\,\rho^{2.41} \quad (7)$$

$$G_{TL,stat}(\rho) = 0.2812\,\rho - 1.7586 \quad (8)$$

$$E_{t,0} = Young´s\ modulus\ parallel\ to\ the\ vascular\ bundles\ [MPa], G_{TL,stat} = static\ shear\ modulus\ TL\ plane\ [MPa], \rho = density\ [\frac{kg}{m^3}]$$

Comparing Young´s modulus and shear modulus, calculated for the average lamella density (379 kg/m³) using dynamic and static relationships, shows overestimations of 152 % (Young´s modulus) and 314 % (shear modulus) by the dynamic relationship. Missing static properties are derived from the dynamic properties by appropriate reduction. Poisson's ratios are not density dependent, the values $\mu_{LT}$ = 0.497, $\mu_{LR}$ = 0.497 and $\mu_{RT}$ = 0.117 are used [13].

# 4. Methods

The following sections present the methods used in this work. The determination of the elastic flexural properties, the selection of modelling parameters and corresponding experiments are illustrated. The implementation of the experiments into the software package RFEM 6.02 is presented.

## 4.1. Determination of the elastic flexural properties according to DIN EN 408:2012-10

The elastic flexural properties are determined according to DIN EN 408:2012-10 [3] in a four-point bending test. The support points are spaced 1836 mm apart, corresponding 18 times the height of the beam (h). The beam length (l) of 2200 mm (21.5 x h) fulfils the requirements given in DIN EN 408:2012-10 [3] (l ≥ 19 x h). Figure 1 shows the corresponding test setup.

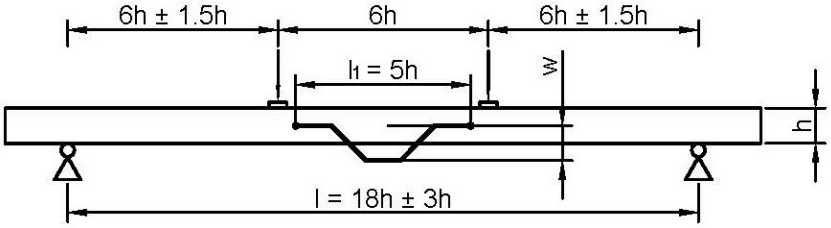


Figure 1: Test setup to determine the flexural properties in a 4-point-bending-test according to DIN EN 408:2012-10 [3]

The distance of the load points equals 6 h (612 mm). In the investigations by Heister [19], these values deviate from the standard with distances of 646 mm, 612 mm and 595 mm. The shortest distance between support and load points is set to 6 ± 1.5 h (459 – 765 mm); distances of 595 mm, 612 mm and 620.5 mm selected by Heister [19] correspond to the specification. Riders may be inserted at the load points to minimise local deformations. Heister [19] uses plywood (beech, birch), pine and oil palm wood riders at load and support points. The applied force must not exceed 0.4 times the estimated maximum force ($F_{max,est}$). Heister [19] assumes 0.4 * $F_{max,est}$ = 1200 N. DIN EN 408:2012-10 [3] distinguishes between local and global MOE. The MOEs correspond to the proportionality constants of the load-deformation curves of the tested beams. The MOEs are determined in the range of 10 % to 40 % of the estimated maximum force. The local MOE is determined using equation (9), the global MOE using equation (10). Due to insufficient data, Heister [19] sets the value for the shear modulus equal to infinity.

$$E_{m,l} = \frac{a l_1^2 (F_2 - F_1)}{16 I (w_2 - w_1)} \quad (9) \qquad E_{m,g} = \frac{3al^2 - 4a^3}{2bh^3 (2\frac{w_2 - w_1}{F_2 - F_1} - \frac{6a}{5Gbh})} \quad (10)$$

$E_{m,l} = local\ MOE\ [MPa], E_{m,g} = global\ MOE\ [MPa], a = smallest\ distance\ support\ to\ load\ point\ [mm], l = distance\ between\ supports\ [mm], l_1 = measuring\ distance\ local\ MOE\ [mm], I = moment\ of\ inertia\ [mm^4], b = beam\ width\ [mm], h = beam\ height\ [mm], F_2 - F_1 = load\ difference\ load\ states\ [N], w_2 - w_1 = deflection\ difference\ states\ [mm], G = shear\ modulus\ [mm]$

## 4.2. Determination of modelling parameters and experiments

The effects of five parameters and their influence on the results of the experiments are investigated. The parameters are the geometry (2D or 3D representation), riders, the material model (isotropic, orthotropic), the material constants determination (non-destructive (nd), destructive (d)) and the element size (8.5 mm, 5.66 mm). Geometry, riders, material model and element size are evaluated to determine parameter settings for further experiments. The investigation of the parameter material properties serves as a starting point for optimisation of the modelling results. Between each experiment one parameter is changed. This makes it possible to observe the parameter effect. The experiments are carried out using 23 beams. The total number of experiments is 138.

## 4.3. Experiment implementation in RFEM 6.02

The experiments are implemented in RFEM 6.02. Geometric modelling, implementation of the support situation, load application and meshing structure are considered. The beams are represented in the form of two- or three-dimensional models. Planes or volume bodies represent the lamellae. A perfect bond is assumed between the lamellae. Modelling of the adhesive joints is omitted in this work, as no failure is reported by Heister [19].
Isotropic and orthotropic linear elastic material models are used to describe the material behaviour of the lamellae. In the isotropic case, one Young´s modulus, one shear modulus and one Poisson's ratio are required. For the Young´s modulus, the Young´s modulus parallel to the vascular bundles is used. The shear modulus is defined by the mean value of the three material specific shear moduli. Young´s and shear modulus are assigned according to the lamella density. The Poisson's ratio is set to $\mu = 0.497$. In the orthotropic case, nine elastic constants are necessary. The Young´s and shear moduli are assigned according to the lamella density using the equations (1) – (6) and the Poisson`s ratios $\mu_{LT} = 0.497$, $\mu_{LR} = 0.497$ and $\mu_{RT} = 0.117$ are used.
The supports are defined as nodal or line supports. No displacement is possible along the Y and Z-axes. The bearings in the X-direction are described by a spring with a spring constant of 0.1 kN/m (see Figure 2) and allow displacements along this axis.

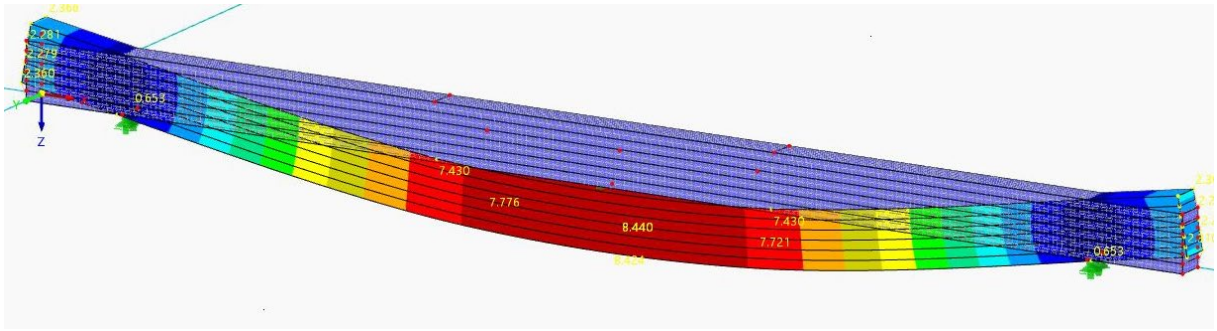


Figure 2: Visual representation of the deformation of specimen A2 (C10)

Four nodal supports are defined to determine the deflection. The supports comply with the specifications in DIN EN 408:2012-10 [3]. Loads are applied in the form of nodal or line loads. The loads act along the Z-axis. Each load point is subjected to half of the total load.
The lamellae are modelled out of rectangular plate elements (2D) or cube-shaped volume elements (3D). The default element size is set to 8.5 mm or 5.66 mm. The element sizes correspond to two, respectively three, elements over the lamella thickness. Riders (experiments 5 and 6) are additional volume bodies in the areas of the support and load points. The riders vary in size, material and material parameters according to Heister [19]. Movement between beam and rider is restricted. The models consist of 3108 elements with 3380 nodes (experiment 1) up to 366019 elements with 110802 nodes (experiment 6).
Deformation and further results, such as equivalent stresses, are calculated using the solver of RFEM 6.02. The results are portrayed as graphical representations (see Figure 2) and nodal displacements in table form.

### 4.4. Determination of the influence of the homogenisation of the lamellae

Natural property gradients are only representable to a limited extend by modelling. The assignment of one density and corresponding material properties to the respective lamella leads to an artificial homogenisation of this lamella. The homogenisation of wood leads to a reduction in the variance of the material properties [21, pp. 681-682]. It can be assumed that the artificial lamella homogenisation shows reduced coefficients of variation (COV). To take effects acting on both specimen groups A and N into account, the quotient of their COVs is calculated (coefficient of comparison (CC)). Changes can be examined by comparing the CCs of the experiments with the CC of Heister [19]. Reduction of the COV of group N with COV of group A leads to an increased value of CC. The CC is calculated according to equation (11).

$$CC = \frac{COV_A}{COV_N} \tag{111}$$

$$CC = comparison\ Coefficient, COV_{A,N} = COV\ specimen\ groups\ A\ and\ N\ [\%]$$

## 5. Results and Discussion

The results of this work are shown and discussed in the following sections. Local and global bending MOE are considered separately and compared afterwards. The influence of shear lamellae density on local and global MOE is investigated. The influence of artificial homogenisation on the specimen collective N is considered. Subsequently, the methods applied and the modelling software used are discussed.

### 5.1. Local MOE

Table 1 shows the statistical variation parameters of the experiments. The local MOE differs between the experiments. The maximum values range from 5603 MPa to 11078 MPa, surrounding the maximum value determined by Heister [19] of 7128 MPa. The minimum values range from 2746 MPa to 8238 MPa and include the minimum of 3151 MPa recorded by Heister [19]. The mean values show the same behaviour as the maximum and minimum values. The highest mean value of 9625 MPa is achieved in experiment 2. The lowest mean value of 4050 MPa is recorded in experiment 6. The mean values of experiments 1 - 3 are about 5350 MPa higher than the mean values of experiments 4 – 6. With 5422 MPa, the mean value of Heister [19] lies in between these two experiment groups. The standard deviations vary between 815 MPa and 864 MPa. The standard deviation of Heister [19] is 1055 MPa and exceeds this range of about 200 MPa. The COVs of experiments 1 - 3 (mean 8.79 %) are 11.66 % below the COVs of experiments 4 – 6 (mean 20.45 %). Heister [19] determines a COV of 19.46 %.

Table 1: Statistical parameters of the local MOE

| | Exp. 1 | Exp. 2 | Exp. 3 | Exp. 4 | Exp. 5 | Exp. 6 | Heister [18] |
|---|---|---|---|---|---|---|---|
| Parameters | 2D, iso, nr nd, 8.5 | 3D, iso, nr, nd, 8.5 | 3D, ortho, nr, nd, 8.5 | 3D, ottho, nr, d, 8.5 | 3D, ortho, r, d, 8.5 | 3D, othro, r, d, 5.66 | |
| MIN [MPa] | 7934 | 8238 | 7961 | 2759 | 2756 | 2746 | 3151 |
| MAX [MPa] | 10848 | 11078 | 10701 | 5768 | 5613 | 5603 | 7128 |
| AVG [MPa] | 9347 | 9625 | 9313 | 4155 | 4051 | 4050 | 5422 |
| SD [MPa] | 838 | 832 | 815 | 864 | 820 | 823 | 1055 |
| COV [%] | 8.97 | 8.64 | 8.75 | 20.78 | 20.23 | 20.32 | 19.46 |

Performing a one-factor ANOVA with repeated measurements provides a p-value of < 2e-16. Tested against a significance level $\alpha = 0.05$, the null hypothesis ($H_0$: mean values local MOE are equal) must be rejected. A posterior pairwise t-test with alpha error correction according to Bonferroni provides the results discussed as follows. P values of 1 result in acceptance of the null hypothesis ($H_0$: mean values are equal). There are no significant differences between experiments 1 and 2, 1 and 3, 2 and 3, 4 and 5, 4 and 6, and 5 and 6. Based on the p-values of < 2e-16, respectively 4e-5, 6.4e-6 and 6.2e-6, the null hypothesis must be rejected for the remaining pairings. Significant differences between the results of Heister [19] and all experiments can be assumed.

Figure 3 on the left shows the relationships between density and local MOEs. Positive linear correlations are given in all experiments. The coefficient of determination $R^2$ of the correlations is between 0.5155 and 0.5492. The slopes of the linear relationships vary between 25.3 and 26.78. The slopes of the experiments differ from the slope of 33.451 given by Heister [19]. Differences between the linear correlations are limited to the ordinate intercept. Due to a deviating slope, the ordinate intercept shows limited comparability with the data from Heister [19].

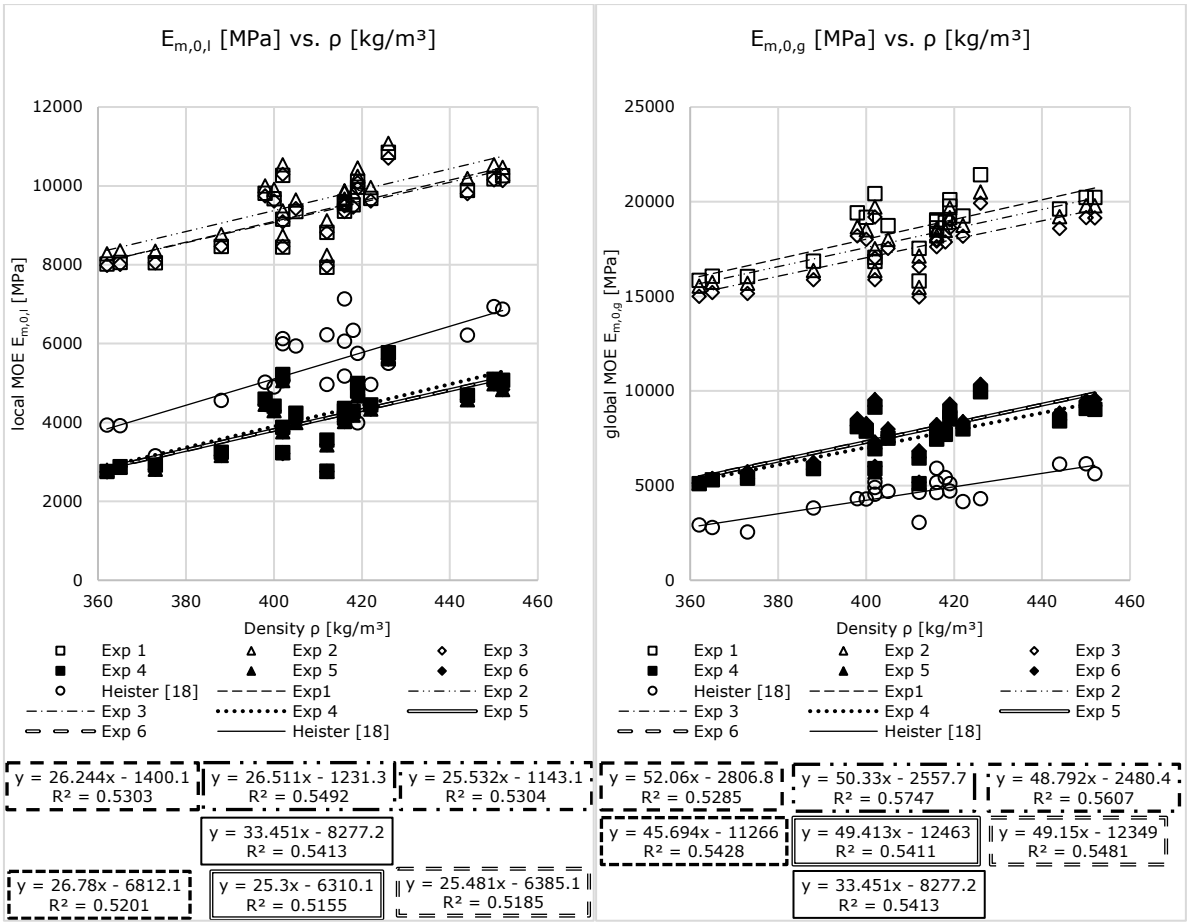


Figure 3: Relationship between density and local MOE (left) respectively global MOE (right) for the six experiments

## 5.2. Global MOE

Table 2 shows the statistical variation parameters of the experiments. The global MOE varies between the experiments. The maximum values range from 9953 MPa to 21414 MPa. The range lies above the maximum value 6142 MPa of Heister [19]. The minimum value 2541 MPa of Heister [19] lies below the range of the experiments from 5092 MPa to 15806 MPa. The mean values show the same behaviour as maximum and minimum values and range from 7447 MPa to 18513 MPa exceeding the mean value 4562 MPa of Heister [19]. The mean values of experiments 1 – 3 are about 10400 MPa higher than of the experiments 4 – 6. The mean values of all experiments exceed the value of Heister [19] by 2885 MPa to 13951 MPa. The standard deviations of the experiments vary between 1442 MPa and 1666 MPa and surpass the standard deviation (1022 MPa) of Heister [19]. The mean COV of experiments 1 – 3 (8.74 %) is 11.03 % lower than the mean COV of experiments 4 – 6 (19.77 %). The COV for Heister [19] is 22.41 % and about 3 % higher than the mean COV of experiments 4 – 6.

Table 2: Statistical parameters of the global MOE

| | Exp. 1 | Exp. 2 | Exp. 3 | Exp. 4 | Exp. 5 | Exp. 6 | Heister [18] |
|---|---|---|---|---|---|---|---|
| MIN [MPa] | 15806 | 15475 | 14955 | 5092 | 5128 | 5128 | 2541 |
| MAX [MPa] | 21414 | 20500 | 19911 | 9953 | 10350 | 10335 | 6142 |
| AVG [MPa] | 18513 | 18053 | 17501 | 7447 | 7773 | 7779 | 4562 |
| SD [MPa] | 1666 | 1544 | 1515 | 1442 | 1562 | 1544 | 1022 |
| COV [%] | 9.00 | 8.55 | 8.66 | 19.37 | 20.10 | 19.85 | 22.41 |

The one-factor ANOVA with repeated measures yields a p-value of < 2e-16. When tested against a significance level $\alpha = 0.05$, the null hypothesis ($H_0$: mean values global MOE are equal) must be rejected. Significant differences between the mean values of the experiments can be assumed. A posterior pairwise t-test with alpha error correction according to Bonferroni delivers a p-value of 0.46 and 1 for the experiment pairings 1 and 2, 1 and 3, 4 and 5, 4 and 6 and 5 and 6. When tested against a significance level $\alpha = 0.05$ the null hypothesis ($H_0$: mean values are equal) needs to be accepted for these pairings. All experiments show significant differences to the results of Heister [19]. Due to p-values < 0.05, the null hypothesis is to be rejected for the remaining pairings. Figure 3 on the right shows the relationships between density and global MOEs. A positive linear relationship between density and global MOE is given in all experiments. The coefficient of determination $R^2$ lies between 0.5285 and 0.5747. The $R^2 = 0.6537$ in the study by Heister [19] is higher. The slopes of the linear correlations vary between 45.694 and 52.06, whereas the slope of Heister [19] with 35.545 is lower. Differences between the linear correlations are mainly limited to the ordinate intercept. Comparison of the ordinate intercepts is only possible to a limited extent due to the deviating slopes.

## 5.3. Discussion of the differences between the experiments for local and global MOE

Differences between the experiments can be attributed to varying factors. The difference between experiments 1 and 2 is the representation dimension (2D, 3D). Limited effects occur based on homogeneous material structure across the beam width. Small differences in the results between experiment 2 and 3 can be attributed to stress distribution in a four-point bending test. The beams are subject to stresses in fibre direction. Ehlbeck *et al.* [14] point out that the Young´s modulus in fibre direction is an influencing factor for bending properties of beams. In experiments 1, 2 and 3 the Young´s modulus along fibre direction is equal. The results vary insignificantly. Riders in experiments 5 and 6 shows no significant effect. This can be attributed to modelling in the elastic range (no plastic deformations). Riders only distribute the load. Minimising the element size shows no significant effect. Glišović *et al.* [22] and Vida *et al.* [23] confirm the sufficient discretisation by two or three elements over the lamella thickness. Significant differences between experiment groups 1 – 3 and 4 – 6 can be attributed to the material parameters. The mean reduction of the Young´s modulus in the fibre direction of 55.4 % corresponds to the mean reduction of the results of the local and global MOE with 56.7 % and 57.5 %.

## 5.4. Comparison local vs. global MOE

The global MOE shows higher values than the local MOE in all experiments. Heister [19] reports an opposite relationship. Smaller global than local MOE is confirmed for spruce by Boström [24]. This relationship is not reported for small global MOEs. Boström [24] describes a transition for the relationship at 10000 MPa (local MOE < global MOE). Nocetti *et al.* [25] confirm a transition for spruce at 8300 MPa. Boström [24] attributes the differences between local and global MOE to shear deformations and the influence of timber defects. The effects described are consistent with the results of experiments 4 – 6. Transferability of the results is limited due to the different materials investigated. The results of Heister [19] and experiments 1 – 3 cannot be explained by the effects described.
The ratio of the mean values of local to global MOE in this investigation ranges from 0.505 to 0.558. The data from Heister [19] provide a ratio of 1.189. Boström [24] reports a ratio of 0.99 for spruce. The values determined by the modelling are below the literature values.

The relationships determined by modelling show high coefficients of determination $R^2$ = 0.9783 – 0.9981. The slopes of the regression lines of the experiments range differ from the slopes of the regression line of Heister [19] and DIN EN 384:2022-08 [26]. The relationship described in DIN EN 384:2022-08 [26] cannot be transferred to oil palm wood based on the present test results.

## 5.5. Influence of the shear lamellae density on the local and global MOE

Deviations of the calculated shear lamellae density from the density ranges provided by Heister [19] justify the investigation of the influence of the shear lamellae density on the local and global MOE. The investigation is carried out using one representative specimen and the modelling approach of experiment 4. Shear lamellae density is varied between 250 kg/m³ and 452 kg/m³. The material constants are varied correspondingly. For both MOEs, a linear relationship between shear lamellae density and the corresponding MOE can be noted. The coefficient of determination of the relationships is $R^2$ = 0.9987 (global MOE) and $R^2$ = 0.9952 (local MOE). An increase in shear lamellae density by 202 kg/m³ corresponds to an increase in the global MOE of 598 MPa (7.7 %) and an increase in the local MOE of 212 MPa (4.7 %). The influence of shear lamella density described here can explain part of the differences between the results of the global MOE of the experiments and Heister [19]. For a more precise determination of the effects, the number of experiments should be increased.

## 5.6. Influence of the homogenisation of the lamellae

Using equation (11), the coefficients of comparison are determined. A CC of 0.6 is recorded for the global MOE in Heister [19]. The CCs of the experiments show values from 0.85 to 0.96. An average increase of 0.31 in the CCs is noted. The comparison of the COVs of specimen groups A with the corresponding value of 14.77 % in Heister [19] shows mean deviations from -6.88 % to 3.45 %. Specimen group N shows deviations from –15.45 % to -3.95 % from the comparative COV of 24.46 %. The observation of increasing CCs and decreasing COVs compared to Heister [19] suggests an influence of artificial homogenisation of the lamellae on the modelling results of specimen group N. For the local MOE, due to the small deviations of the CCs of maximum 4.7 % in connection with small deviations of the COV, an effect of artificial homogenisation cannot be proven.

## 5.7. Discussion of methods and modelling software

The software RFEM 6.02 can be considered suitable for modelling the flexural behaviour of oil palm glulam. The modelling results differ from comparative laboratory tests. The differences are attributed to the material constants used. An optimization of the results is possible by adjusting the material constants. The material constants and the methods for material constant adjustment show limited applicability. The use of dynamically determined material constants leads to significant overestimations of local and global MOE, the use of corrected elastic properties leads to significant differences from the comparative tests. The parameter settings of the experiments are suitable for representing the tests carried out by Heister [19]. The depiction of the support and load represent reality with sufficient accuracy. The results show no significant difference between two and three-dimensional geometry models. Two-dimensional geometry models can be used to reduce computational effort. Changing the material model from isotropic to orthotropic shows no significant effect on the test results. Riders do not show influences on the experiments. The element sizes used show no significant influence on the modelling results. The reduction of the element size leads to a significant increase of the calculation time. The use of two elements over the lamella thickness is recommended.
The release date of RFEM 6.02 is recent at the time of writing. Inconveniences using RFEM can be noted. It is not possible to add user defined materials to the material library. Materials need to be created anew for each model. Importing material data from external sources (e.g. Excel files) is restricted. It is possible to control RFEM using programming languages, for example Python. This interface does not allow for the creation and saving of user-defined materials. Geometric models can be created via a graphical user interface or table input. Both variants are suitable for creating easy geometric models. The import

of CAD data can be realised to a limited extent. More exact modelling of property gradients in oil palm wood cannot be implemented in RFEM. The assignment of separate material properties to individual elements cannot be implemented. An adjustment of the mesh structure is possible to a limited extent. Finally, it can be stated that RFEM 6.02 is suitable for the modelling in the context of this work.

# 6. Conclusion and Outlook

The results of the experiments confirm the applicability of FEM for modelling oil palm wood-based glulam. The geometric models, volume and plane models based on individual layers with varying material properties, are suitable to represent the comparative tests. The investigation of the factors model dimension, material model, riders, material parameter determination and element size show no significant influence on the modelling results, the material parameter determination. The results of this work show significant deviations from laboratory tests, which can be attributed to the elastic constants used. Further investigations need to be carried out to guarantee reliable input parameters. The correlations between density and local and global MOE shown in this work are comparable to laboratory tests. Adjustments of the material parameters can be used to optimize the results. The comparison of the local and global MOE shows deviating behaviour from literature for common wood species. The global MOE exceeds the local MOE in all experiments. Further investigations on the global MOE of oil palm glulam are necessary and can use the findings of this work. The shear lamella density shows influences on the local and global MOE. Further experiments are needed to consolidate this influence. An influence of artificial homogenisation of lamellae on the results of the global MOE can be demonstrated (specimens N). RFEM 6.02 is suitable for the modelling carried out in the context of this work. Negative aspects include difficult input of user defined materials and limited usability of software interfaces. RFEM 6.02 can be used and recommended to a limited extent for modelling of complex structures and material inhomogeneity. The results of this work offer starting points for further modelling investigations. Considerations of the bending strength of glulam, realistic representation of inhomogeneous material structures and optimisation of results themselves and of investigated products are field of further investigations.

# 7. Acknowledgements

The investigation was financed by the German Federal Ministry of Education and Research through the «Bioökonomie International 2017» project «Oilpalmsugar (031B0767A)».

# 8. References

[1] Food and Agriculture Organization of the United Nations. «Crops and livestock products.» https://www.fao.org/faostat/en/#data/QCL (accessed Jun. 3, 2022).

[2] A. Fruehwald and K. Fruehwald-Koenig, «The Use of Oil Palm Trunks for Wood Products,» in *By-Products of Palm Trees and Their Applications*, 2019, pp. 69–80, doi: 10.21741/9781644900178-3.

[3] DIN Deutsches Institut für Normung e. V., *DIN EN 408:2012-10 Holzbauwerke – Bauholz für tragende Zwecke und Brettschichtholz – Bestimmung einiger physikalischer und mechanischer Eigenschaften; Deutsche Fassung EN 408:2010+A1:2012*.

[4] DIN Deutsches Institut für Normung e. V., *DIN EN 14080:2013-09 Holzbauwerke – Brettschichtholz und Balkenschichtholz – Anforderungen; Deutsche Fassung EN 14080:2013*.

[5] W. Killmann and S. C. Lim, «Anatomy and properties of oil palm stem,» in *Proceedings NATIONAL SYMPOSIUM OF OIL PALM BY-PRODUCTS*, Kuala Lumpur, Forest Research Institute Malyasia (FRIM), Ed., vol. 87, 1985, pp. 1–25.

[6] S. C. Lim and K. C. Khoo, «Characteristics of oil palm trunk and its potential utilization,» *Malaysian Forest*, vol. 49, pp. 3–22, 1986.

[7] N. Kölli, «Density and Moisture Distribution in Oil Palm Trunks from Peninsular Malaysia,» Bachelor-Thesis, University of Hamburg, Hamburg, 2016a.

[8] L. Fathi, «Structural and mechanical properties of the wood from coconut palms, oil palms and date palms,» Doctoral Thesis, University of Hamburg, Hamburg, 2014.

[9] K. Fruehwald-Koenig, «Properties and Grading of Oil Palm Lumber,» in *Proceedings: 21st International Nondestructive Testing and Evaluation of Wood Symposium.*, Freiburg, X. Wang, U. H. Sauter, and R. J. Ross, Eds., 2019, pp. 204–212.

[10] K. Fruehwald-Koenig and L. Heister, «Macromechanical and Micromechanical Behavior of Oil Palm Wood (Elaeis guineensis JACQ.) – Part 1: Tensile, Compression and Bending Properties,» *Publication in preparation*, 2022.

[11] N. Kölli, «Relation shear modulus and densitiy for oil palm wood (Elaeis guineensis JACQ.),» *Personal communication*, 2022b.

[12] K. Fruehwald-Koenig and B. Faust, «Evaluation of Elastic Constants of Oil Palm Wood using Ultrasonic Measurement,» in *Proceedings: 22st International Nondestructive Testing and Evaluation of Wood Symposium.*, Quebec City, Canada, X. Wang and R. J. Ross, Eds., 2022, pp. 29–39.

[13] M. Hackel, «Bestimmung der Querdehnungszahlen von Ölpalmenholz (Elaeis guineensis Jacq.) im Druckversuch parallel zur Faser an Probekörpern in Gebrauchsabmessungen,» Scientific Internship, Ostwestfalen-Lippe University of Applied Sciences and Arts, Lemgo, 2022.

[14] J. Ehlbeck, F. Colling, and R. Görlacher, «Einfluß keilgezinkter Lamellen auf die Biegefestigkeit von Brettschichtholzträgern,» *Holz als Roh-und Werkstoff*, vol. 43, no. 8, pp. 333–337, 1985, doi: 10.1007/BF02607817.

[15] H. J. Blaß, J. Denzler, M. Frese, P. Glos, and P. Linsemann, *Biegefestigkeit von Brettschichtholz aus Buche* (Karlsruher Berichte zum Ingenieurholzbau 1). Universitätsverlag Karlsruhe, 2005.

[16] M. Frese and H. J. Blaß, «Characteristic bending strength of beech glulam,» *Mater Struct*, vol. 40, no. 1, pp. 3–13, 2007, doi: 10.1617/s11527-006-9117-9.

[17] Y. Gao, Y. Wu, X. Zhu, L. Zhu, Z. Yu, and Y. Wu, «Numerical Analysis of the Bending Properties of Cathay Poplar Glulam,» *Materials (Basel, Switzerland)*, early access. doi: 10.3390/ma8105362.

[18] E. Ferrier, P. Labossière, and K. W. Neale, «Modelling the bending behaviour of a new hybrid glulam beam reinforced with FRP and ultra-high-performance concrete,» *Applied Mathematical Modelling*, vol. 36, no. 8, pp. 3883–3902, 2012, doi: 10.1016/j.apm.2011.11.062.

[19] L. Heister, «Untersuchung des Einflusses der Rohdichte auf die Biegeeigenschaften von Ölpalme (Elaeis guineensis Jacq.),» Master-Thesis, Ostwestfalen-Lippe University of Applied Sciences and Arts, Lemgo, 2020.

[20] DIN Deutsches Institut für Normung e. V., *DIN EN 338:2016-07 Bauholz für tragende Zwecke – Festigkeitsklassen; Deutsche Fassung EN 338:2016*.

[21] F. Kollmann, *Technologie des Holzes und der Holzwerkstoffe: Anatomie und Pathologie, Chemie, Physik, Elastizität und Festigkeit,* 2nd ed. Springer Berlin Heidelberg, 1951.

[22] I. Glišović, M. Pavlović, B. Stevanović, and M. Todorović, «Numerical analysis of glulam beams reinforced with CFRP plates,» *Journal of Civil Engineering and Management*, vol. 23, no. 7, pp. 868–879, 2017, doi: 10.3846/13923730.2017.1341953.

[23] C. Vida, M. Lukacevic, J. Eberhardsteiner, and J. Füssl, «Modeling approach to estimate the bending strength and failure mechanisms of glued laminated timber beams,» *Engineering Structures*, vol. 255, p. 113862, 2022, doi: 10.1016/j.engstruct.2022.113862.

[24] L. Boström, «Determination of the modulus of elasticity in bending of structural timber - comparison of two methods,» *Holz als Roh-und Werkstoff*, vol. 57, no. 2, pp. 145–149, 1999, doi: 10.1007/s001070050030.

[25] M. Nocetti, L. Brancheriau, M. Bacher, M. Brunetti, and A. Crivellaro, «Relationship between local and global modulus of elasticity in bending and its consequence on structural timber grading,» *Holz als Roh-und Werkstoff*, vol. 71, no. 3, pp. 297–308, 2013, doi: 10.1007/s00107-013-0682-7.

[26] DIN Deutsches Institut für Normung e. V., *DIN EN 384:2022-08 Bauholz für tragende Zwecke – Bestimmung charakteristischer Werte für mechanische Eigenschaften und Rohdichte; Deutsche Fassung EN 384:2016+A2:2022*.